

Geophysical Research Letters®

RESEARCH LETTER

10.1029/2022GL099183

Key Points:

- Gravity field and Steady-State Ocean Circulation Explorer (GOCE) gravity mission detected signals of upper crust in the Tibetan Plateau, which reveals the decoupled folding of the lithosphere
- The decoupled folding process provides an alternative explanation of Tibetan Plateau's anomalously thick crust and flat topography
- Our 3D viscoelastic numerical modeling explains the wavelenths of the decoupled folding beneath the Tibetan Plateau

Supporting Information:

Supporting Information may be found in the online version of this article.

Correspondence to:

Y. H. Shin and B.-D. So,
yhshin@kigam.re.kr;
bdso@kangwon.ac.kr

Citation:

Shin, Y. H., Shum, C. K., Braitenberg, C., Lee, S. M., Lim, M., Na, S.-H., et al. (2022). Decoupled lithospheric folding, lower crustal flow channels, and the growth of Tibetan Plateau. *Geophysical Research Letters*, 49, e2022GL099183. <https://doi.org/10.1029/2022GL099183>

Received 6 MAY 2022
 Accepted 25 JUN 2022

Decoupled Lithospheric Folding, Lower Crustal Flow Channels, and the Growth of Tibetan Plateau

Young Hong Shin^{1,2}, C. K. Shum^{2,3} , Carla Braitenberg⁴ , Sang Mook Lee⁵ , Mutaek Lim¹, Sung-Ho Na⁶ , Chunli Dai⁷ , Chaoyang Zhang⁸ , Yuanjin Pan⁹ , Seok-Hyeon Do¹⁰ , and Byung-Dal So¹⁰ 

¹Korea Institute of Geosciences and Mineral Resource, Daejeon, Korea, ²Division of Geodetic Science, School of Earth Sciences, Ohio State University, Columbus, OH, USA, ³Innovation Academy for Precision Measurement Science and Technology, Chinese Academy of Sciences, Wuhan, China, ⁴Department of Mathematics and Geosciences, University of Trieste, Trieste, Italy, ⁵School of Earth & Environmental Sciences, Seoul National University, Seoul, Korea, ⁶University of Science and Technology, Daejeon, Korea, ⁷Department of Civil and Environmental Engineering, Louisiana State University, Baton Rouge, LA, USA, ⁸Center for Space Research, The University of Texas at Austin, Austin, TX, USA, ⁹State Key Laboratory of Information Engineering in Surveying, Mapping and Remote Sensing, Wuhan University, Wuhan, China, ¹⁰Department of Geophysics, Kangwon National University, Gangwon-do, Korea

Abstract The growth mechanism of the Tibetan Plateau, postulated by a number of hypotheses, remains under intense debate. Our analysis of recent satellite-based gravity model reveals that Tibetan lithosphere has been decoupled and folded. It is further evidenced by the existence of crustal melts and channel flow that have been observed by seismic and magnetotelluric explorations. Based on 3D geodynamic simulations, we elucidate the exact buckling structures in the upper crust and lithospheric mantle: at mixed wavelengths between ~240 and ~400 km, the lower crustal viscosity is smaller than $\sim 10^{19}$ Pa-s, implicating weak lower crustal flow beneath the Plateau. This mixed wavelength is consistent with the result of our inverse gravity modeling. Our results facilitate a new plausible hypothesis that the decoupled lithospheric folding mechanism can explain the growth mechanism of the anomalously thick and wide Tibetan Plateau by conflating our idea and contemporary hypothesized scientific findings.

Plain Language Summary The Tibetan Plateau, known as the Roof of the World, is the highest and largest Plateau on Earth, whose formation involves complex and active geodynamic processes since the Late Miocene. Here we emphasize the importance of decoupled lithospheric folding and its geodynamic process that has not yet been fully considered in the contemporary hypotheses on the origin of Tibetan Plateau's formation. The deep-seated folding structure modeled using the latest satellite gravimetry shows a structure consistent with the plate tectonic setting, which allows rocks to melt easier and flow in the lower crust underneath the Tibetan Plateau. Our hypothesis was further tested and validated by three-dimensional numerical simulations, revealing the decoupled lithospheric folds in the collisional tectonic setting. Our study is consistent with the existence of partial melting and flow channels of the Tibetan lower crust previously discovered by geophysical explorations. Further it makes it easier to explain the morphological characteristics, magma of crustal origin, and in particular, the mass transport process in the lower crust, which is the most important factor in the formation processes of the Tibetan Plateau, than the indentation process of the strong lithosphere.

1. Introduction

The Tibetan Plateau is a unique geophysical feature due to its extreme size and elevation, and is one of the most geologically active regions in the world with unique climatic and geodynamic processes. Modern geodetic, geophysical, and geological observations reveal that the Tibetan Plateau is subjected to the collisional environment between India and Eurasia tectonic plates, and is still undergoing convergent movement (Pan et al., 2018). However, there is no definitive consensus elucidating the growth process of the Plateau, which would completely explain the outstanding findings, including the extraordinary thick crust and subducting slabs (Zhao et al., 2010), widely spread crustal melts and channel flows (Bai et al., 2010; Nelson et al., 1996; Unsworth et al., 2005; Wei et al., 2001), lithospheric folding structure (Jin et al., 1994; Shin et al., 2009, 2015), and magmatism (Chung et al., 2005; Ding et al., 2003). Alternatively, ad hoc mechanisms including an oblique stepwise NE progressive growth model (Tapponnier et al., 2001) have been suggested to explain some aspects of the growth process

and to interpret new scientific observations, based on existing hypotheses including: (a) stacking and shortening (Allégre et al., 1984), (b) underthrusting of India (Argand, 1924; Ni & Barazangi, 1984), (c) injecting and hydraulic uplifting (Zhao & Morgan, 1985), (d) continental extrusion (Harrizon et al., 1992; Molnar & Tapponnier, 1975), and (e) possible lower crustal flow (Royden et al., 1997).

Lithospheric folding has not yet been considered as an essential constraint in the postulated formation mechanisms of the Tibetan Plateau, although the possibility of existence of the decoupled folding was first suggested by Jin et al. (1994), and subsequently refined to include the development of a three-dimensional (3D) Moho folding (Shin et al., 2009). However, the lithospheric folding in response to compressional stress is a much more widespread mode of deformation than previously thought (Cloetingh et al., 1999). It is possible that folding played an important role on basin formation (Cloetingh & Burov, 2011), as well as on the production of magmatism in certain locations (Shin et al., 2012). The buckling structure can rise as a result of tectonic compressional situation in which a mechanically strong layer is sandwiched by weaker medium (Hobbs et al., 2008). In this scenario, the strong region at the brittle-ductile transition zone hosts a buckling structure.

Previous numerical studies investigated the correlation between lithospheric rheology and buckling structures (Gerbault, 2000). Strength envelopes of continental lithospheres show at least two local strength maximum at the center of upper crust and the top of lithospheric mantle (Burov, 2011), which indicates that more than two buckling can grow simultaneously under compression. Analog and numerical studies (Currie et al., 1962; Schmid & Podladchikov, 2006) suggested that the interaction of two buckling structures is highly nonlinear, depending on a distance between two strong layers and strength of medium. In this study, we performed 3D viscoelastic geodynamic simulations based on Lagrangian finite element method to examine the effects of lower crustal viscosity on the degree of decoupling between two buckling structures.

According to our analysis, detectable signals from the decoupled interfaces between three layers of upper and lower crust and upper mantle can be found. In addition, the 3D investigation of the lower crustal structure indicates that pressure variation due to the folding is very likely related to the regions of crustal melts which had been observed by seismic and magnetotelluric (MT) explorations. These studies support the idea that the buckling-induced pressure decrease has increased the melting possibility of lower crust, partially mixed with bottom of upper crust and top of lithospheric mantle as well as the existence of lower crustal melts and their flow channel. In the decoupled lithospheric folding model, the channel flow is not limited to the boundary regions but can be extended to inside the whole Plateau, which facilitates the crustal mass supplies into the interior of the Plateau, supporting the growth of the Plateau into an abnormally high, wide, and flat feature. Such explanation can in turn link the mechanical lithospheric folding process to the crust-originated magmatism at collisional regions.

2. Methods

We applied the methodology described in our former studies (Shin et al., 2007, 2009) for upward continuation, the gravity effect of topography and sediments, spectral analyses, gravity inversion, and Moho fold estimation. Coherence and coherency analysis and effective elastic thickness estimation is based on Forsyth method (Forsyth, 1985).

In numerical simulation, the size of three-dimensional domain is $2,000 \times 2,000 \times 297$ km (Figure S1 in Supporting Information S1). The spatial scale is consistent with the Tibet and its associated numerical studies (Chen et al., 2017; Li et al., 2013). To investigate viscoelastic behaviors associated with buckling of upper crust and lithospheric mantle, we adopted COMSOL Multiphysics® (ver. 5.4) to solve a coupled system of quasi-static momentum conservation equation (Equation 1) and Maxwell viscoelastic constitutive relation (Equation 2).

$$\frac{\partial \sigma_{ij}}{\partial x_j} = 0 \quad (j = 1, 2, 3) \quad (1)$$

$$\dot{\epsilon}'_{ij} = \dot{\epsilon}'_{ij}{}^E + \dot{\epsilon}'_{ij}{}^V = \frac{1}{2G} \frac{D\sigma'_{ij}}{Dt} + \frac{\sigma'_{ij}}{2\eta} \quad (i, j = 1, 2, 3) \quad (2)$$

σ_{ij} and x_j are Cauchy's stress tensor and spatial coordinates, respectively. Deviatoric strain-rate tensor $\dot{\epsilon}'_{ij}$ is the sum of deviatoric elastic strain-rate $\dot{\epsilon}'_{ij}{}^E$ and viscous strain-rate $\dot{\epsilon}'_{ij}{}^V$ tensors. G , D/Dt , t , σ'_{ij} , and η are, respectively, shear modulus, material derivative, time, deviatoric stress tensor, and viscosity.

Our layered models have four layers, that is, upper crust, lower crust, strong lithospheric mantle, and weak upper mantle. The upper crust and lithospheric mantle play the role of a strong core for initiating the buckling mode between free-surface and lower crust and between lower crust and weak upper mantle, respectively. The viscosity profile (Figure S2 in Supporting Information S1) has been widely used to simplify temperature-dependent strength envelopes with two brittle-ductile transition zones in upper crust and lithospheric mantle (e.g., Bischoff & Flesch, 2018; Keum & So, 2021). The detailed values of mechanical properties of each layer are displayed in Table S1 of Supporting Information S1.

To initiate the buckling instability, we applied a small-scale sinusoidal perturbation, which has ~ 0.01 km amplitude and ~ 200 km wavelength, to the lower crust (Figure S3 in Supporting Information S1). We adopted free slip boundary condition to bottom and east-west (EW) side walls. The top surface is free surface to mimic a sharp strength contrast between air and upper crust. The north-south (NS) compression is simulated by constant strain-rate boundary condition of $5 \cdot 10^{-16} \text{ s}^{-1}$ at the both of north and south side boundaries. The bulk shortening is up to $\sim 5\%$. Previous semi-analytical and numerical studies suggested that $< 10\%$ shortening is sufficient for fully grown buckling instability (Zhang et al., 1996). Total degree of freedom reached ~ 3 millions. We used Multifrontal Massively Parallel sparse direct Solver (Amestoy et al., 2000) to solve momentum equation.

3. Data Analysis

Gravity data analyzed in this study is the most recently released global gravity model by the European Space Agency, GO_CONS_GCF_2_DIR_R6 (Förste et al., 2019), in short, DIR_R6. Spectral analysis of the gravity model shows that DIR_R6 can recover the spatial resolution up to 156 km (spherical harmonics, or SH, complete to degree and order 256), while the signals gradually decrease up to 140 km (SH degree 286) in the study area (Figure 1). Observed coherence between Bouguer anomaly (BA) and topography matches well for effective elastic thickness (T_e) of 37 km. It is evident that the correlation between the observed and predicted is much better than the earlier gravity models used in prior studies (Jin et al., 1994; Shin et al., 2007), which illustrates the improvement of the gravity model including new data and analysis methods. The coherence curve shows an unexpected pattern for wavelengths shorter than 156 km. It shows a peak at around 110 km, which was previously interpreted as a buried load (Shin et al., 2007). However, we now attribute the peak to an artifact induced by error in the interpolation, and to the topography data of 30 arc-minutes resolution for BA computation. This is because that this signal is beyond the spatial resolution limit of Gravity field and Steady-State Ocean Circulation Explorer (GOCE). Thus the same anomalous pattern (but reduced amplitude) of Earth Gravitational Model 1996 (Lemoine et al., 1998) could be caused by similar error source, because the topography-based predicted gravity data was used for the wide area where no-terrestrial gravity data are available in Tibet (Shin et al., 2007). Formerly a terrestrial-gravity-based study also showed a very similar pattern and attributed the pattern as evidence for not being a single elastic lithosphere (Jin et al., 1994). However, the noted correlation at about 110 km could originate from the inclusion of geophysically predicted data. Therefore, for the study of large-scale Tibetan crust and lithosphere deformation, the use of the satellite-only gravity model is preferable than using higher resolution combination gravity models in which the less accurate or interpolated terrestrial gravity and/or topography data were used.

The Shuttle Radar Topography Mission data (Becker et al., 2009; Farr et al., 2007) is used for computing gravity effect caused by topography in determining of BA and for computing Moho depth of Airy-type isostasy as well. We also estimated the effect of the sedimentary basin by using the 30 arc-minute sedimentary thickness data from the Institute of Geodesy and Geophysics, Chinese Academy of Science (Shin et al., 2007). Density model in this study is determined by considering the seismic-exploration-based density model of Haines et al. (2003). It divided the crust into six layers for Lhasa and Qiangtang blocks. A jump in density is appeared between the third and fourth layers. Based on the model, we determined the density of topography as $2,570 \text{ kg/m}^3$, sedimentary $2,465 \text{ kg/m}^3$, upper crust $2,691 \text{ kg/m}^3$, lower crust $3,044 \text{ kg/m}^3$, and upper mantle $3,412 \text{ kg/m}^3$. As we divided the crust into two layers, we used weighted mean of three layers of upper and lower layers. Only we modified the density of upper mantle as $3,412 \text{ kg/m}^3$ instead of $3,320 \text{ kg/m}^3$, because the former gives better fitting of the

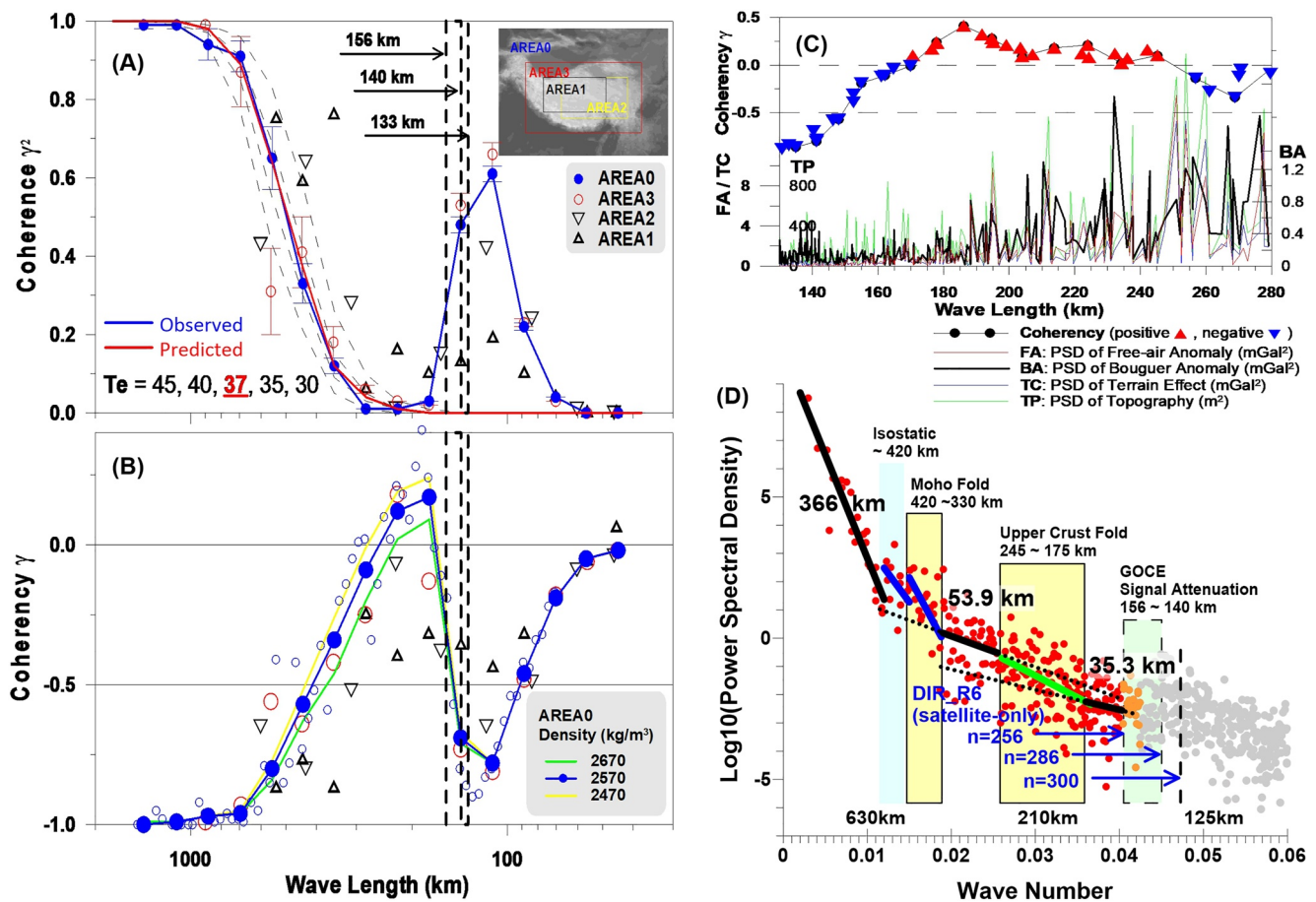


Figure 1. Spectral analysis: (a) The coherence of Bouguer anomaly (BA) and topography shows that the Tibetan lithosphere has effective elastic thickness (T_e) of about 37 km. (b) Coherence shows positive at wavelengths between 175 and 245 km, while negative at the others. (c) BA has positive coherence with topography, which is presumed to represent the late stage of upper crustal folding (Figure 2(c)). (d) Power spectral analysis of BA shows three density discontinuities of 366 km, 53.9 km, and 35.3 km, which are corresponding to 410-km discontinuity marking the top of the mantle transition zone, Moho, and the boundary between upper and lower crust, respectively. Anomalous patterns are shown in waves corresponding to upper crustal fold (green line), Moho fold, and partial isostatic deformation (blue lines).

Moho of gravity inversion with that of seismic explorations. The calculated BA (Figure S4 in Supporting Information S1), representing anomalous subsurface mass distribution, shows some large differences with that of Shin et al. (2015) along the southern boundary of the Tibetan Plateau. However, it is not due to the observed gravity but due to the difference of the topography models, because there are only small differences of N-S directional stripe pattern between the gravity models of DIR_R6 (used in this study) and DIR_R5 (used by Shin et al. (2015)).

Gravity inversion primarily depends on the signal separation for the target interface of density contrast. BA, having peaks at 175–245 km and positive coherence (Figure 1c), could be interpreted as upper crustal fold signals, associated with the late stage of folding process (Figure 2c), while BA having peaks 330–420 km has been interpreted as Moho fold signals (Shin et al., 2009). If the wavelengths are assumed to be those of the Moho fold rather than upper crustal fold, it would not be in agreement with the predicted folding wavelengths of an elastic plate of T_e 37 km. Such an argument can be made because the prevailing folding wavelength would be 384 km for a continental lithosphere of T_e 37 km, and 205 km for much smaller T_e of 16 km (Shin et al., 2009). With the corresponding wavelengths the mean depth is also estimated as 28.3 km ((35.3–7.0) km), that is, the expected depth for the boundary between upper and lower crust (Figure 1d). Thus we separate the signals into two parts: one generated at the deep interface, that is, Moho and its folds, those having the most of the signals longer than 300 km, and the other from shallower interface, that is, folds that lie at boundary between upper and lower crust, having signals between 175 and 245 km.

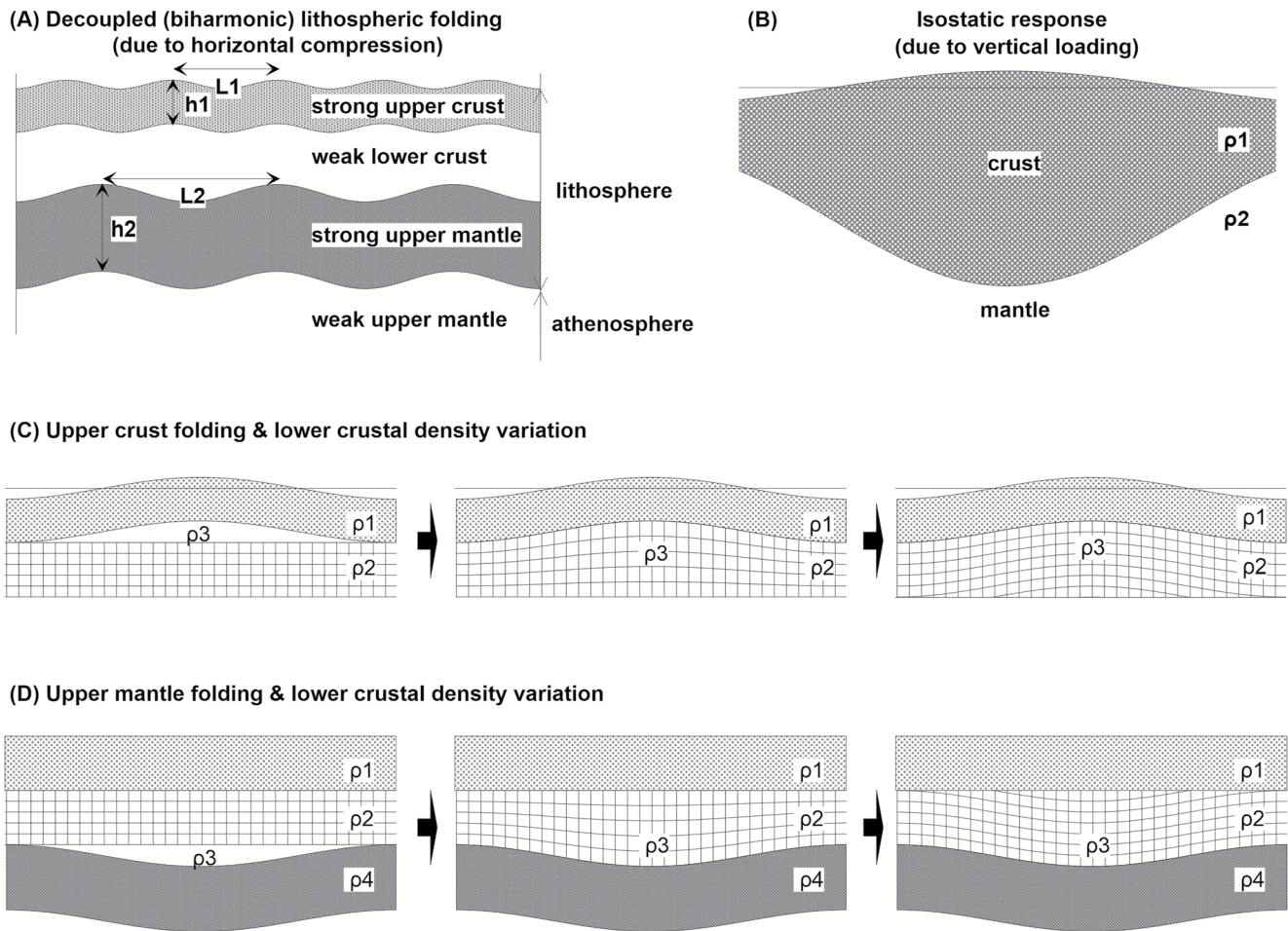


Figure 2. Basic concept of the decoupled lithospheric folding for gravity data analysis: In compressional tectonic setting, the lithosphere could have both folding component (a) and isostatic component (b). If an elastic upper crust, underlain by a ductile lower crust, is folded due to compression, lower crustal density (ρ_3) could vary from the early to late stages along with the mass flow. Accordingly, the coherency between Bouguer anomaly (BA) and topography varies from negative to positive (c). If an elastic upper mantle lithosphere is folded, the overlying lower crustal density could also vary as time goes on. However, the coherency would not be clear, because the topography deformation is depending on the rheology of the layers, while the BA has clearly shifted to negative (d). The meshes represent density, that is, each block has same mass. At the beginning of decoupling, density ρ_3 is assumed to be almost 0 and then increase up to nearly as much as ρ_2 . It is also assumed that density increases with depth: upper crust (ρ_1) < lower crust (ρ_2) < upper mantle (ρ_4).

4. Results and Discussion

4.1. Subsurface Structure and Lithospheric Folding

Crust structure is calculated by using the so-called Parker-Oldenburg method using the fast Fourier transform algorithm. The estimated Moho structure reveals a very thick crust and three “Moho ranges” (Shin et al., 2007) beneath the Plateau (Figure S6 in Supporting Information S1). Moho undulation along the west and east lines best fit with seismic explorations when the density contrast of 368 kg/m^3 and mean depth of 46.9 km. The fold structure of Moho could be estimated by eliminating the isostatic component from the whole Moho undulation (Shin et al., 2009), assuming that the Moho structure has two kinds of components: one is a folding component due to horizontal loading in the compressional tectonic environment, and the other an isostatic component due to vertical loading (Figure 2). The estimated Moho fold structure (Figure S7 in Supporting Information S1) exhibits the EW and NS directionality which is in agreement with the observed crustal velocity derived from the global positioning system (GPS) observations (Pan et al., 2018). The prevailing wavelengths are at 330, 342, 374, 405, and 417 km, whose values are close to that of the predicted, 384 km. Coherency of the Moho folding components would become negative with time, since the lithosphere would be unable to support the vertical loading of the corresponding wavelengths and consequently undergoes deformation due to isostatic response.

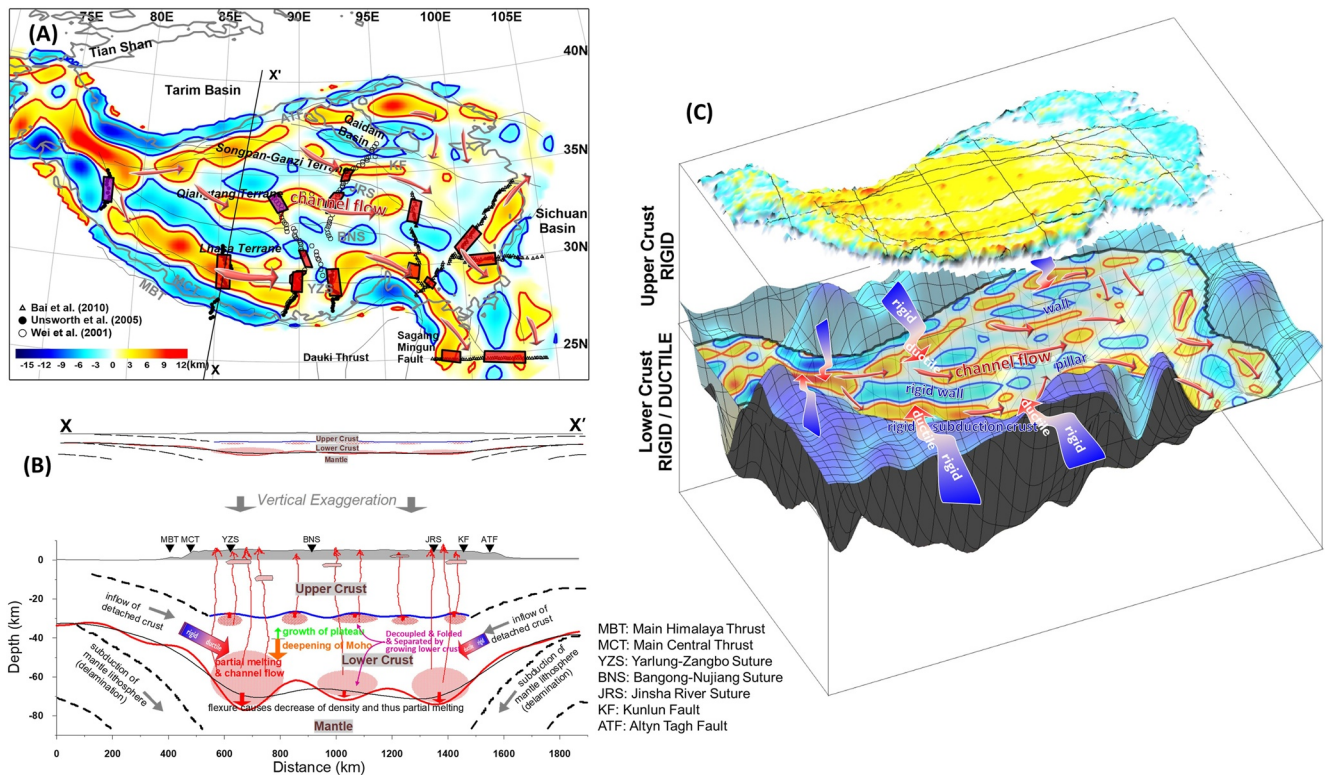


Figure 3. Vertical inflation of the lower crust (a) and the schematic illustration of the hypothesis of the decoupled-lithospheric-folding-based plateau growing (b), (c): The inflation of lower crust (red regions) corresponds to the locations of the partial melts or channel flows (rectangles or polygons with shaded red (strong conductivity) and purple (less strong conductivity)) observed by magnetotelluric (MT) surveys. It means that the density decrease due to the decoupled folding could have played an important role on the melting and viscous channel flowing at lower crust, which is slowly moving between rigid walls or pillars (blue regions). It might shed light on 3D distribution of the channel flow, extending the 2D channel flow suggested by the results of the MT explorations. Red and blue contours represent ± 2 km to emphasize the ductile and rigid regions, respectively. Melting along subducting slabs and of deeper mantle origin is not considered here. Gray line bordering the Plateau represents 3-km-height level.

The upper crustal folding that lies at the boundary between upper and lower crust is estimated with the BA of wavelengths between 175 and 245 km (Figure S8 in Supporting Information S1), while the other wavelengths are filtered out even if they might reflect the boundary structure between upper and lower crust since they are not thought to be associated with the upper crustal folding. The directionality is very similar with that of the Moho fold, except for the unexpected NS directionality in the western end of Lhasa terrane. This could be explained if there was an intermediate EW stress on Lhasa Terrane for a certain period in the past (not observed by present-day GPS, e.g., Chung et al., 2005) that was strong enough to fold the upper crust but was not strong enough to fold the mantle lithosphere. Our crustal folding model indicates that there could be another decoupled shallow layer at the top of the upper crust in southeastern Tibet, as the GPS shows quite different direction of surface mass flow from that of the subsurface folding structures. The superimposed effect of the complex geology of fault zones can be further investigated with terrestrial gravity data of higher resolution.

Our analysis shows that the GOCE gravity model has recovered the signals from the two separated folding structures beneath the Tibetan Plateau. Thus a decoupled (biharmonic) folding model is more likely to explain the observed feature than a coupled (monoharmonic) folding model (Cloetingh et al., 1999; Jin et al., 1994). It appears that the weak lower crust, a layer sandwiched between the two, must have experienced volume (pressure) change proportional to the folding and uplift/subsidence rate of the upper crust above and the upper mantle below. The volume inflation calculated with the decoupled lithospheric folding model (Figure 3a) shows that it is consistent with the distribution of partial melts or channel flows observed by seismic and MT explorations (Bai et al., 2010; Unsworth et al., 2005; Wei et al., 2001). We argue that the

decrease of pressure due to the decoupled folding process has greatly influenced the lower crustal melting and viscous channel flowing (red regions in Figure 3a). The flow would be slowly moving between rigid walls or pillars (blue regions in Figure 3a). This effect would be largest at the early stage of the decoupled folding, because the uplift/subsidence rate may have been the largest at the early stage of folding process and but decreased with time (Shin et al., 2012).

4.2. Mechanics of Decoupled Buckling

We performed 3D numerical simulations to test our hypothesis. The initial thickness of lower crust is 47 km similar to our gravity inverse modeling. Previous studies argued that the Tibet was simultaneously thickened with the India-Eurasia collision (e.g., Chung et al., 2009). However, England and Searle (1986) suggested that the thickening occurred prior to the collision to explain the reduced shortening rate after the collision using the positive buoyancy from 3–5 km uplifted Lhasa Block (52.5–70 km crustal thickness). Figure 4 shows the interaction between the two buckling structures with different values of lower crustal viscosity. We selected this lower crustal viscosity following previous geophysical studies (Clark et al., 2005; Copley et al., 2011). Figures 4a and 4b exhibit the buckling and topography for the cases of $\sim 10^{19}$ Pa·s and $\sim 10^{20.5}$ Pa·s viscosity of lower crust after 4.7% shortening. The decoupled buckling appeared in Figure 4a. The two buckling structures in upper crust and lithospheric mantle display different wavelength of ~ 240 and ~ 400 km, respectively. This pattern of buckling indicates that the two structures preserve their inherent buckling modes. On the other hand, when the lower crustal viscosity is as high as $10^{20.5}$ Pa·s (Figure 4b), our simulation results show a single wavelength (i.e., ~ 480 km) of the two buckling in upper crust and lithospheric mantle, which cannot constrain the observation. The multiple and mixed waveform of buckling are similar with our gravity anomaly observation, which infers that lower crust viscosity beneath the Tibet is as low as 10^{19} Pa·s.

In the bottom row of Figure 4, we also present the negative and positive dynamic pressure using red and blue colors, respectively. The deviation in dynamic pressure is ~ 100 MPa, indicating the small-scale expansion and contraction of the lower crust occurred during buckling growth. The concept of dynamic pressure has been widely adopted for the mechanisms of deep-focused earthquakes (So & Yuen, 2015), fluid/melt transport in the subducting slab (Gerya, 2015). Moreover, we found that the magmatism and volume inflation by folding are spatially correlated (see Figure 3a). We speculate that the dynamic pressure changes due to buckling can be associated with localized partial melting and magmatism. We note that our models are built on viscoelastic solid mechanics in which the mantle convection is not considered. The compressional thickening can cause lithospheric delamination (Chen, 2021; Kim & So, 2020), which affects the buckling mode.

5. Conclusions

We suggest that the decoupled folding has played a key role in the growth of the Tibetan Plateau (Figure 3); mass supplies into the Tibetan lower crust from the detached crust of the subducting slab have been revealed by seismic imagings (Nelson et al., 1996; Owens & Zandt, 1997). If a sufficient melting condition has been reached by the pressure decrease due to the decoupled lithospheric folding, the mass inflow from the outside crust would be much easier with less resistance, and the slowly moving viscous channel flow could supply mass into the interior of the entire plateau. Then, with the growth of the Plateau, the crust isostatically deepened. Therefore, one could explain the reason why the Plateau has grown so high, wide, and flat. It further explains the decrease of convergence rate (Lee & Lawver, 1995) and the growth rate of the Plateau as well, because the resistance against the mass inflow increases as uplift/subsidence rate of the folding process decreases with time (Shin et al., 2012).

Contemporary and multiple satellite geodetic sensors have demonstrated their ability of delineating various geodynamical- meteorological- cryospheric processes on the Earth's surface and its interior. With longer observation records from these geodetic sensors, and the complementary use of traditional geophysical methods, including seismic, MT, and terrestrial gravity surveys, it would be increasingly plausible to further constrain the outstanding hypotheses on the theory of the growth of the Tibetan Plateau.

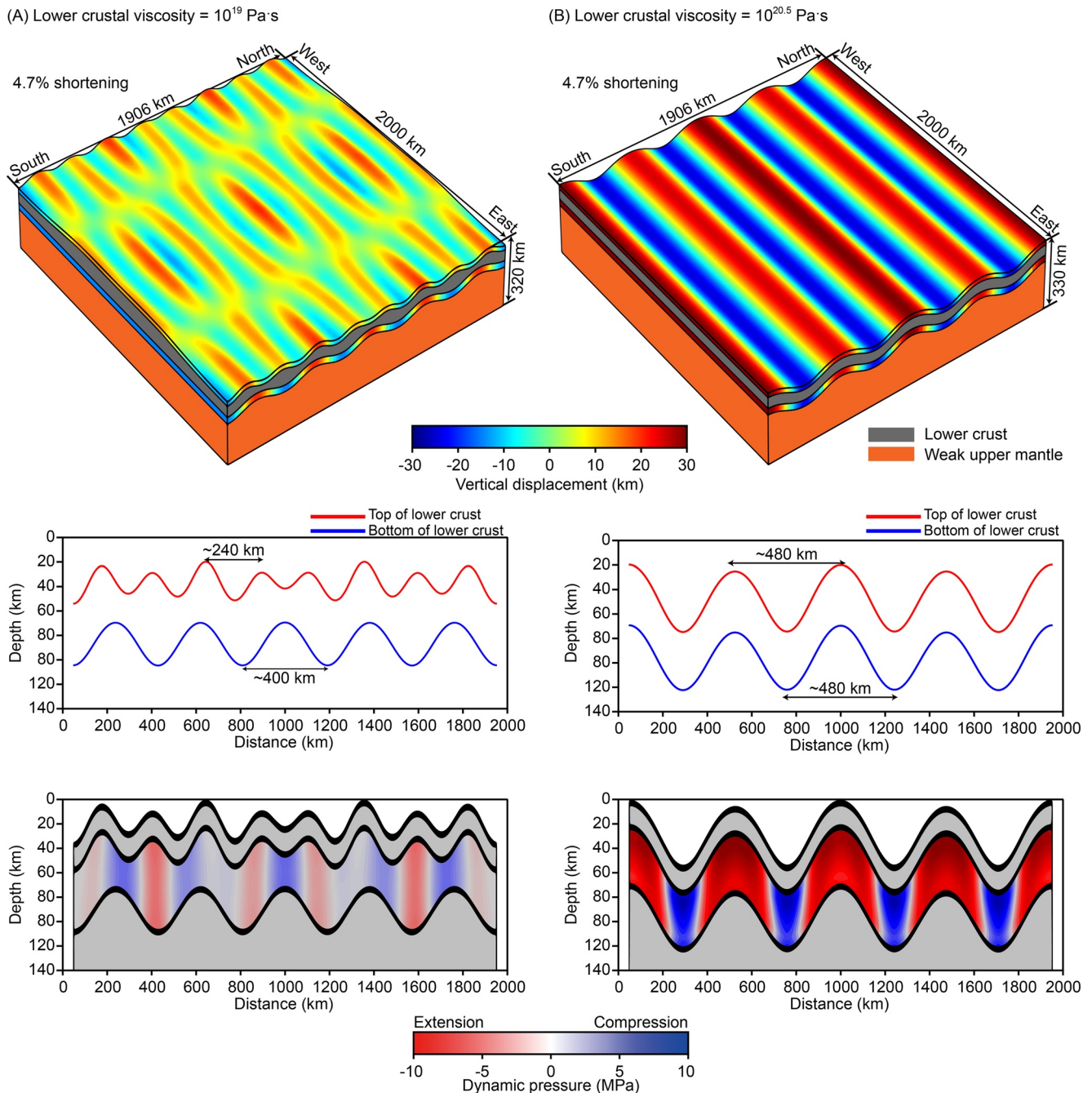


Figure 4. (a) Decoupled and (b) fully-coupled buckling structures after $\sim 5\%$ shortening. For (a) and (b), we applied $\sim 10^{19}$ Pa·s and $\sim 10^{20.5}$ Pa·s viscosity to lower crust, respectively. The top row in (a) and (b) shows folded shapes of each layer. Gray and orange colors refer to lower crust and weak upper mantle, respectively. The rainbow colors on the top, front, and east surfaces indicate the vertical displacement measured in upper crust and lithospheric mantle, respectively. The topographies along top (red lines) and bottom (blue lines) of lower crust in the middle row in (a) and (b). In the bottom row, dynamic pressure in the lower crust induced by buckling is displayed.

Data Availability Statement

The gravity inversion results are available in a Zenodo repository (<https://doi.org/10.5281/zenodo.6635298>). They are computed from gravity data provided on ICGEM webpage (<http://icgem.gfz-potsdam.de/home>).

Acknowledgments

We thank Dr. Lin Chen and an anonymous reviewer for their constructive comments which have improved the manuscript. This research is partially supported by National Key Research & Development Program of China (2017YFA0603103). Y. H. was supported by the Basic Research Projects (22-3116 & 22-3211) of KIGAM. S.-H. and B.-D. are supported by National Research Foundation of Korea, 2019R1A6A1A03033167 and 2022R1A2C1009742.

References

Allégre, C. J., Courtillot, V., Tapponnier, P., Hirn, A., Mattauer, M., Coulon, C., et al. (1984). Structure and evolution of the Himalaya-Tibet orogenic belt. *Nature*, 307(5946), 17–22. <https://doi.org/10.1038/307017a0>

Amestoy, P. R., Duff, I. S., & L'Excellent, J. Y. (2000). Multifrontal parallel distributed symmetric and unsymmetric solvers. *Computer Methods in Applied Mechanics and Engineering*, 184(2–4), 501–520. [https://doi.org/10.1016/S0045-7825\(99\)00242-X](https://doi.org/10.1016/S0045-7825(99)00242-X)

Argand, E. (1924). La tectonique de l'Asie. In *Proceedings of the 13th international geological congress* (Vol. 7, pp. 171–372).

Bai, D., Unsworth, M. J., Meju, M. A., Ma, X., Teng, J., Kong, X., et al. (2010). Crustal deformation of the eastern Tibetan plateau revealed by magnetotelluric imaging. *Nature Geoscience*, 3(5), 358–362. <https://doi.org/10.1038/ngeo830>

Becker, J. J., Sandwell, D. T., Smith, W. H. F., Braud, J., Binder, B., Depner, J., et al. (2009). Global bathymetry and elevation data at 30 arc seconds resolution: SRTM30_Plus. *Marine Geodesy*, 32(4), 355–371. <https://doi.org/10.1080/01490410903297766>

Bischoff, S. H., & Flesch, L. M. (2018). Normal faulting and viscous buckling in the Tibetan Plateau induced by a weak lower crust. *Nature Communications*, 9(1), 4952. <https://doi.org/10.1038/s41467-018-07312-9>

Burov, E. B. (2011). Rheology and strength of the lithosphere. *Marine and Petroleum Geology*, 28(8), 1402–1443. <https://doi.org/10.1016/j.marpetgeo.2011.05.008>

Chen, L. (2021). The role of lower crustal rheology in lithospheric delamination during orogeny. *Frontiers of Earth Science*, 9, 755519. <https://doi.org/10.3389/feart.2021.755519>

Chen, L., Capitanio, F. A., Liu, L., & Gerya, T. V. (2017). Crustal rheology controls on the Tibetan plateau formation during India-Asia convergence. *Nature Communications*, 8(1), 15992. <https://doi.org/10.1038/ncomms15992>

Chung, S., Chu, M., Ji, J., O'Reilly, S. Y., Pearson, N. J., Liu, D., et al. (2009). The nature and timing of crustal thickening in Southern Tibet: Geochemical and zircon Hf isotopic constraints from postcollisional adakites. *Tectonophysics*, 477(1), 36–48. <https://doi.org/10.1016/j.tecto.2009.08.008>

Chung, S.-L., Chu, M.-F., Zhang, Y., Xie, Y., Lo, C.-H., Lee, T.-Y., et al. (2005). Tibetan tectonic evolution inferred from spatial and temporal variations in post-collisional magmatism. *Earth-Science Reviews*, 68(3–4), 173–196. <https://doi.org/10.1016/j.earscirev.2004.05.001>

Clark, M. K., Bush, J. W. M., & Royden, L. H. (2005). Dynamic topography produced by lower crustal flow against rheological strength heterogeneities bordering the Tibetan Plateau. *Geophysical Journal International*, 162(2), 575–590. <https://doi.org/10.1111/j.1365-246X.2005.02580.x>

Cloetingh, S., & Burov, E. (2011). Lithospheric folding and sedimentary basin evolution: A review and analysis of formation mechanisms. *Basin Research*, 23(3), 257–290. <https://doi.org/10.1111/j.1365-2117.2010.00490.x>

Cloetingh, S., Burov, E., & Poliakov, A. (1999). Lithosphere folding: Primary response to compression? (from central Asia to Paris basin). *Tectonics*, 18(6), 1064–1083. <https://doi.org/10.1029/1999TC900040>

Copley, A., Avouac, J., & Wernicke, B. P. (2011). Evidence for mechanical coupling and strong Indian lower crust beneath southern Tibet. *Nature*, 472(7341), 79–81. <https://doi.org/10.1038/nature09926>

Currie, J. B., Patnode, H. W., & Trump, R. P. (1962). Development of folds in sedimentary strata. *The Geological Society of America Bulletin*, 73(6), 655–673. [https://doi.org/10.1130/0016-7606\(1962\)73\[655:DOFISS\]2.0.CO;2](https://doi.org/10.1130/0016-7606(1962)73[655:DOFISS]2.0.CO;2)

Ding, L., Kapp, P., Zhong, D., & Deng, W. (2003). Cenozoic volcanism in Tibet: Evidence for a transition from oceanic to continental subduction. *Journal of Petrology*, 44(10), 1833–1865. <https://doi.org/10.1093/ptrology/egg061>

England, P., & Searle, M. (1986). The Cretaceous-tertiary deformation of the Lhasa Block and its implications for crustal thickening in Tibet. *Tectonics*, 5(1), 1–14. <https://doi.org/10.1029/TC0051001p00001>

Farr, T. G., Rosen, P. A., Caro, E., Crippen, R., Duren, R., Hensley, S., et al. (2007). The shuttle radar topography mission. *Review of Geophysics*, 45(2), RG2004. <https://doi.org/10.1029/2005RG000183>

Förster, C., Abrykosov, O., Bruinsma, S., Dahle, C., König, R., & Lemoine, J.-M. (2019). ESA's Release 6 GOCE gravity field model by means of the direct approach based on improved filtering of the reprocessed gradients of the entire mission. GFZ Data Services. <https://doi.org/10.5880/ICGEM.2019.004>

Forsyth, D. W. (1985). Subsurface loading and estimates of the flexural rigidity of continental lithosphere. *Journal of Geophysical Research*, 90(B14), 12623–12632. <https://doi.org/10.1029/JB090iB14p12623>

Gerbault, M. (2000). At what stress level is the central Indian Ocean lithosphere buckling? *Earth and Planetary Science Letters*, 178(1–2), 165–181. [https://doi.org/10.1016/S0012-821X\(00\)00054-6](https://doi.org/10.1016/S0012-821X(00)00054-6)

Gerya, T. (2015). Tectonic overpressure and underpressure in lithospheric tectonics and metamorphism. *Journal of Metamorphic Geology*, 33(8), 785–800. <https://doi.org/10.1111/jmg.12144>

Haines, S. S., Klempner, S. L., Brown, L., Jingru, G., Mechie, J., Meissner, R., et al. (2003). INDEPTH III seismic data: From surface observations to deep crustal processes in Tibet. *Tectonics*, 22(1), 1001. <https://doi.org/10.1029/2001TC001305>

Harrison, T. M., Copeland, P., Kidd, W. S. F., & Yin, A. (1992). Raising Tibet. *Science*, 255(5052), 1663–1670. <https://doi.org/10.1126/science.255.5052.1663>

Hobbs, B., Regenauer-Lieb, K., & Ord, A. (2008). Folding with thermal–mechanical feedback. *Journal of Structural Geology*, 30(12), 1572–1592. <https://doi.org/10.1016/j.jsg.2009.03.014>

Jin, Y., McNutt, M. K., & Zhu, Y.-S. (1994). Evidence from gravity and topography data for folding of Tibet. *Nature*, 371(6499), 669–674. <https://doi.org/10.1038/371669a0>

Keum, J.-Y., & So, B.-D. (2021). Effect of buoyant sediment overlying subducting plates on trench geometry: 3D viscoelastic free subduction modeling. *Geophysical Research Letters*, 48(9), e2021GL093498. <https://doi.org/10.1029/2021gl093498>

Kim, D., & So, B.-D. (2020). Effects of rheology and mantle temperature structure on edge-driven convection: Implications for partial melting and dynamic topography. *Physics of the Earth and Planetary Interiors*, 303, 106487. <https://doi.org/10.1016/j.pepi.2020.106487>

Lee, T.-Y., & Lawver, L. A. (1995). Cenozoic plate reconstruction of Southeast Asia. *Tectonophysics*, 251(1–4), 85–138. [https://doi.org/10.1016/0040-1951\(95\)00023-2](https://doi.org/10.1016/0040-1951(95)00023-2)

Lemoine, F. G., Kenyon, S. C., Factor, J. K., Trimmer, R. G., Pavlis, N. K., Chinn, D. S., et al. (1998). The development of the joint NASA GSFC and the national imagery and mapping agency (NIMA) geopotential model EGM96. NASA/TP-1998-206861.

Li, Z., Xu, Z., Gerya, T., & Burg, J. (2013). Collision of continental corner from 3-D numerical modeling. *Earth and Planetary Science Letters*, 380, 98–111. <https://doi.org/10.1016/j.epsl.2013.08.034>

Molnar, P., & Tapponnier, P. (1975). Cenozoic tectonics of Asia: Effects of a continental collision. *Science*, 189(4201), 419–426. <https://doi.org/10.1126/science.189.4201.419>

Nelson, K. D., Zhao, W., Brown, L. D., Kuo, J., Che, J., Liu, X., et al. (1996). Partially molten middle crust beneath southern Tibet: Syn-thesis of Project INDEPTH results. *Sciences*, 274(5293), 1684–1688. <https://doi.org/10.1126/science.274.5293.1684>

- Ni, J., & Barazangi, M. (1984). Seismotectonics of the Himalayan collision zone: Geometry of the underthrusting Indian plate beneath the Himalaya. *Journal of Geophysical Research*, 89(B2), 1147–1163. <https://doi.org/10.1029/JB089IB02P01147>
- Owens, T. J., & Zandt, G. (1997). Implications of crustal property variations for models of Tibetan plateau evolution. *Nature*, 387(6628), 37–42. <https://doi.org/10.1038/387037a0>
- Pan, Y., Shen, W.-B., Shum, C. K., & Chen, R. (2018). Spatially varying surface seasonal oscillations and 3-D crustal deformation of the Tibetan Plateau derived from GPS and GRACE data. *Earth and Planetary Science Letters*, 502, 12–22. <https://doi.org/10.1016/j.epsl.2018.08.037>
- Royden, L. H., Burchfiel, B. C., King, R. W., Wang, E., Chen, Z., Shen, F., & Liu, Y. (1997). Surface deformation and lower crustal flow in eastern Tibet. *Science*, 276(5313), 788–790. <https://doi.org/10.1126/science.276.5313.788>
- Schmid, D. W., & Podladchikov, Y. Y. (2006). Fold amplification rates and dominant wavelength selection in multilayer stacks. *Philosophical Magazine*, 86(21–22), 3409–3423. <https://doi.org/10.1080/14786430500380175>
- Shin, Y. H., Choi, K. S., Koh, J.-S., Yun, S.-H., Nakamura, E., & Na, S.-H. (2012). Lithospheric-folding-based understanding on the origin of the back-arc basaltic magmatism beneath Jeju volcanic island. *Tectonics*, 31(4), TC4005. <https://doi.org/10.1029/2011tc003092>
- Shin, Y. H., Shum, C.-K., Braitenberg, C., Lee, S. M., Na, S.-H., Choi, K. S., et al. (2015). Moho topography, ranges and folds of Tibet by analysis of global gravity models and GOCE data. *Scientific Reports*, 5(1), 11681. <https://doi.org/10.1038/srep11681>
- Shin, Y. H., Shum, C. K., Braitenberg, C., Lee, S. M., Xu, H., Choi, K. S., et al. (2009). 3D fold structure of the Tibetan Moho from GRACE gravity data. *Geophysical Research Letters*, 36(1), L01302. <https://doi.org/10.1029/2008GL036068>
- Shin, Y. H., Xu, H., Braitenberg, C., Fang, J., & Wang, Y. (2007). Moho undulations beneath Tibet from GRACE-integrated gravity data. *Geophysical Journal International*, 170(3), 971–985. <https://doi.org/10.1111/j.1365-246X.2007.03457.x>
- So, B.-D., & Yuen, D. A. (2015). Generation of tectonic over-pressure inside subducting oceanic lithosphere involving phase-loop of olivine-wadsleyite transition. *Earth and Planetary Science Letters*, 413, 59–69. <https://doi.org/10.1016/j.epsl.2014.12.048>
- Tapponnier, P., Xu, Z., Roger, F., Meyer, B., Arnaud, N., Wittlinger, G., & Jingsui, Y. (2001). Oblique stepwise rise and growth of the Tibet plateau. *Science*, 294(5547), 1671–1677. <https://doi.org/10.1126/science.105978>
- Unsworth, M. J., Jones, A. G., Wei, W., Marquis, G., Gokarn, S. G., & Spratt, J. E. (2005). Crustal rheology of the Himalaya and Southern Tibet inferred from magnetotelluric data. *Nature*, 438(7064), 78–81. <https://doi.org/10.1038/nature04154>
- Wei, W., Unsworth, M., Jones, A., Booker, J., Tan, H., Nelson, D., et al. (2001). Detection of widespread fluids in the Tibetan crust by magnetotelluric studies. *Science*, 292(5517), 716–719. <https://doi.org/10.1126/science.1010580>
- Zhang, Y., Hobbs, B. E., Ord, A., & Mühlhaus, H. B. (1996). Computer simulation of single-layer buckling. *Journal of Structural Geology*, 18(5), 643–655. [https://doi.org/10.1016/S0191-8141\(96\)80030-7](https://doi.org/10.1016/S0191-8141(96)80030-7)
- Zhao, J., Yuan, X., Liu, H., Kumar, P., Pei, S., Kind, R., et al. (2010). The boundary between the Indian and Asian tectonic plates below Tibet. *Proceedings of the National Academy of Sciences of the United States of America*, 107(25), 11229–11233. <https://doi.org/10.1073/pnas.1001921107>
- Zhao, W.-L., & Morgan, W. J. (1985). Uplift of Tibetan plateau. *Tectonics*, 4, 359–369. <https://doi.org/10.1029/TC004i004p00359>

References From the Supporting Information

- Gan, W., Zhang, P., Shen, Z.-K., Niu, Z., Wang, M., Wan, Y., et al. (2007). Present-day crustal motion within the Tibetan Plateau inferred from GPS measurements. *Journal of Geophysical Research*, 112(B8), B08416. <https://doi.org/10.1029/2005JB004120>
- Kreemer, C., Blewitt, G., & Klein, E. C. (2014). A geodetic plate motion and global strain rate model. *Geochemistry, Geophysics, Geosystems*, 15(10), 3849–3889. <https://doi.org/10.1002/2014GC005407>